A&A 562, A119 (2014)
DOI: 10.1051/0004-6361/201322140

Astronomy & Astrophysics

Vacuum-UV spectroscopy of interstellar ice analogs

I. Absorption cross-sections of polar-ice molecules⋆

G. A. Cruz-Diaz[1], G. M. Muñoz Caro[1], Y.-J. Chen[2,3], and T.-S. Yih[3]

[1] Centro de Astrobiología, INTA-CSIC, Carretera de Ajalvir, km 4, Torrejón de Ardoz, 28850 Madrid, Spain
e-mail: [cruzdga; munozcg]@cab.inta-csic.es
[2] Space Sciences Center and Department of Physics and Astronomy, University of Southern California, Los Angeles, CA 90089-1341, USA
[3] Department of Physics, National Central University, Jhongli City, 32054 Taoyuan Country, Taiwan

Received 25 June 2013 / Accepted 15 December 2013

ABSTRACT

Context. The vacuum-UV (VUV) absorption cross sections of most molecular solids present in interstellar ice mantles with the exception of H_2O, NH_3, and CO_2 have not been reported yet. Models of ice photoprocessing depend on the VUV absorption cross section of the ice to estimate the penetration depth and radiation dose, and in the past, gas phase cross section values were used as an approximation.
Aims. We aim to estimate the VUV absorption cross section of molecular ice components.
Methods. Pure ices composed of CO, H_2O, CH_3OH, NH_3, or H_2S were deposited at 8 K. The column density of the ice samples was measured in situ by infrared spectroscopy in transmittance. VUV spectra of the ice samples were collected in the 120−160 nm (10.33−7.74 eV) range using a commercial microwave-discharged hydrogen flow lamp.
Results. We provide VUV absorption cross sections of the reported molecular ices. Our results agree with those previously reported for H_2O and NH_3 ices. Vacuum-UV absorption cross section of CH_3OH, CO, and H_2S in solid phase are reported for the first time. H_2S presents the highest absorption in the 120−160 nm range.
Conclusions. Our method allows fast and readily available VUV spectroscopy of ices without the need to use a synchrotron beamline. We found that the ice absorption cross sections can be very different from the gas-phase values, and therefore, our data will significantly improve models that simulate the VUV photoprocessing and photodesorption of ice mantles. Photodesorption rates of pure ices, expressed in molecules per absorbed photon, can be derived from our data.

Key words. astrochemistry – ultraviolet: ISM – ISM: molecules – instrumentation: spectrographs – methods: laboratory – techniques: photometric

1. Introduction

Ice mantles in dense cloud interiors and cold circumstellar environments are composed mainly of H_2O and other species such as CO_2, CO, CH_4, CH_3OH, and NH_3 (Mumma & Charnley 2011, and references therein). Some species with no permanent or induced dipole moment, such as O_2 and N_2, cannot be easily observed in the infrared, but are also expected to be present in the solid phase (e.g., Ehrenfreund & van Dishoeck 1998). The relative to water abundances of the polar species CO, CH_3OH, and NH_3 are between 0−100%, 1−30%, and 2−15%. In comets the abundances are 0.4−30%, 0.2−7%, 0.2−7%, and ∼0.12−1.4% for CO, CH_3OH, NH_3, and H_2S (Mumma & Charnley 2011, and references therein). We therefore included H_2S in this study because this reduced species was detected in comets and is expected to form in ice mantles (Jiménez-Escobar & Muñoz Caro 2011). In the coldest regions where ice mantles form, thermally induced reactions are inhibited. Therefore, irradiation processes by UV-photons or cosmic rays may play an important role in the formation of new species in the ice and contribute to the desorption of ice species to the gas phase. Cosmic rays penetrate deeper into the cloud interior than UV-photons, generating secondary UV-photons by excitation of H_2 molecules. This secondary UV-field will interact more intensively with the grain mantles than direct impact by cosmic rays (Cecchi-Pestellini & Aiello 1992; Chen et al. 2004). VUV photons have the power to excite or dissociate molecules, leading to a complex chemistry in the grains. The VUV-region encloses wavelengths from 200 nm to about 100 nm, since the term extreme-ultraviolet (EUV) is often used for shorter wavelengths.

The estimation of the VUV-absorption cross sections of molecular ice components allows one to calculate the photon absorption of icy grains in that range. In addition, the VUV-absorption spectrum as a function of photon wavelength is required to study the photodesorption processes over the full photon emission energy range. Photoabsorption cross-section measurements in the VUV-region were performed for many gas phase molecules. Results for small molecules in the gas phase were summarized by Okabe (1978), but most of these cross-section measurements for molecular bands with fine structure are severely distorted by the instrumental bandwidths (Hudson & Carter 1968). The integrated cross sections are less affected by the instrumental widths, and approach the true cross sections as optical depth approaches zero. Therefore, the true integrated cross section can be obtained from series of data taken with different column densities (Samson & Ederer 2000).

The lack of cross-section measurements in solids has led to the assumption that the cross sections of molecules in ice mantles were similar to the gas phase values. In recent years the VUV-absorption spectra of solid H_2O, CH_3OH, NH_3, CO_2,

⋆ Data can be found at http://ghosst.osug.fr/

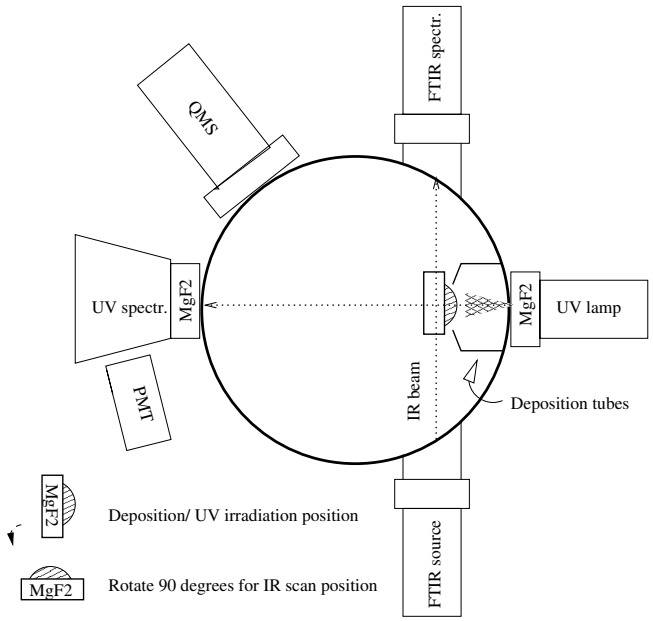

Fig. 1. Scheme of the main chamber of ISAC. The VUV-light intersects three MgF_2 windows before it enters the UV-spectrometer, but the emission spectrum that the ice experiences corresponds to only one MgF_2 window absorption, the one between the VUV-lamp and the ISAC main chamber. FTIR denotes the source and the detector used to perform infrared spectroscopy. QMS is the quadrupole mass spectrometer used to detect gas-phase species. PMT is the photomultiplier tube that makes the ultraviolet spectroscopy possible.

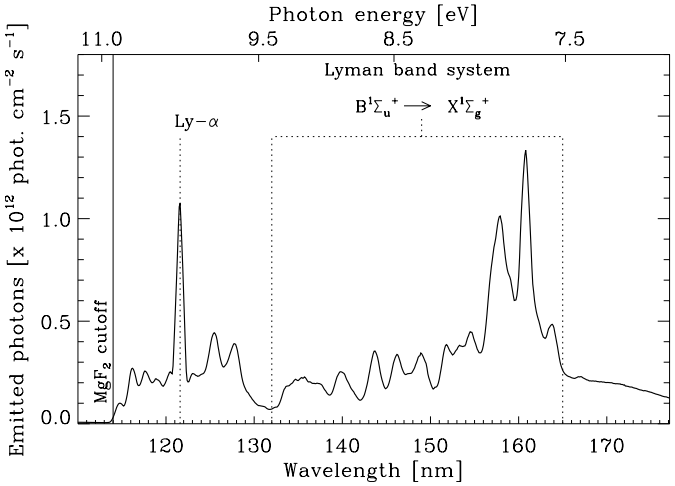

Fig. 2. UV-photon flux as a function of wavelength of the MDHL in the 110 to 170 nm range estimated with the total photon flux calculated using actinometry. The spectrum corresponds to a measurement with one MgF_2 window intersecting the emitted VUV-light cone. This spectrum is the one experienced by the ice sample. The VUV-emission is dominated by the Ly-α peak (121.6 nm) and the Lyman band system.

O_2, N_2, and CH_4 were reported by Mason et al. (2006), Kuo et al. (2007), and Lu et al. (2008). But the VUV-absorption cross sections were only estimated for solid H_2O, NH_3, and CO_2 (Mason et al. 2006). Furthermore, all previous works have been performed using synchrotron monochromatic light as the VUV-source, scanning the measured spectral range.

In the present work, we aim to provide accurate measurements of the VUV-absorption cross sections of interstellar ice polar components including H_2O, CH_3OH, NH_3, CO, and H_2S. The use of a hydrogen VUV-lamp, commonly used in ice irradiation experiments, limits the spectroscopy to the emission range between 120 and 160 nm, but this has several advantages: the measurements are easy to perform and can be made regularly in the laboratory, without the need to use synchrotron beam time. A second paper will be dedicated to the nonpolar molecular ice components including CO_2, CH_4, N_2, and O_2. In Sect. 2 the experimental protocol is described. Section 3 provides the determination of VUV-absorption cross sections for the different ice samples. The astrophysical implications are presented in Sect. 4. The conclusions are summarized in Sect. 5.

2. Experimental protocol

The experiments were performed using the interstellar astrochemistry chamber (ISAC), see Fig. 1. This set-up and the standard experimental protocol were described in Muñoz Caro et al. (2010). ISAC mainly consists of an ultra-high-vacuum (UHV) chamber, with pressure typically in the range $P = 3–4.0 \times 10^{-11}$ mbar, where an ice layer made by deposition of a gas species onto a cold finger at 8 K, achieved by means of a closed-cycle helium cryostat, can be UV-irradiated. The evolution of the solid sample was monitored with in situ transmittance FTIR spectroscopy and VUV-spectroscopy. The chemical components used for the experiments described in this paper were H_2O(liquid), triply distilled; CH_3OH(liquid), Panreac Química S. A. 99.9%; CO(gas), Praxair 99.998%; NH_3(gas), Praxair 99.999%; and H_2S(gas), Praxair 99.8%. The deposited ice layer was photoprocessed with an F-type microwave-discharged hydrogen flow lamp (MDHL), from Opthos Instruments. The source has a VUV-flux of $\approx 2 \times 10^{14}$ cm^{-2} s^{-1} at the sample position, measured by $CO_2 \rightarrow CO$ actinometry, see Muñoz Caro et al. (2010). The Evenson cavity of the lamp is refrigerated with air. The VUV-spectrum is measured routinely in situ during the irradiation experiments with the use of a McPherson 0.2 m focal length VUV monochromator (model 234/302) with a photomultiplier tube (PMT) detector equipped with a sodium salicylate window, optimized to operate from 100–500 nm (11.27–2.47 eV), with a resolution of 0.4 nm. The characterization of the MDHL spectrum has been studied before by Chen et al. (2010) and will be discussed in more detail by Chen et al. (2013).

The interface between the MDHL and the vacuum chamber is a MgF_2 window. The monochromator is located at the rear end of the chamber, separated by another MgF_2 window. This means that the measured background spectra, that is without an ice sample intersecting the VUV-light cone, are the result of the radiation that intersects two MgF_2 windows.

Grating corrections were made for the VUV-spectra in the range of 110–180 nm (11.27–6.88 eV). The mean photon energy was calculated for the spectrum corresponding to only one MgF_2 window intersecting the VUV-lamp emission, since that is the mean photon energy that the ice sample experiences. This one-window spectrum, displayed in Fig. 2, was measured by directly coupling the VUV-lamp to the spectrometer with a MgF_2 window acting as the interface. The proportion of Ly-α in 110–180 nm range is 5.8%, lower than the 8.4% value estimated by Chen et al. (2013). This difference could be due to the lower transmittance of the MgF_2 window used as interface between the MDHL and the UHV-chamber, although the different position of the pressure gauge measuring the H_2 flow in the MDHL may also play a role.

It was observed that most of the energy emitted by the VUV-lamp lies below 183 nm (6.77 eV) and the MgF_2 window cutoff

occurs at 114 nm (10.87 eV). The mean photon energy in the 114−180 nm (10.87−6.88 eV) range is $E_{\rm photon}$ = 8.6 eV. The main emission bands are Ly-α at 121.6 nm (10.20 eV) and the molecular hydrogen bands centered on 157.8 nm (7.85 eV) and 160.8 nm (7.71 eV) for a hydrogen pressure of 0.4 mbar, see Fig. 2.

3. VUV-absorption cross section of interstellar polar ice analogs

We recorded VUV-absorption spectra of pure ices composed of CO, H_2O, CH_3OH, NH_3, and H_2S. For each ice spectrum a series of three measurements was performed: i) the emission spectrum of the VUV-lamp was measured to monitor the intensity of the main emission bands; ii) the emission spectrum transmitted by the MgF_2 substrate window was measured to monitor its transmittance; and iii) the emission spectrum transmitted by the substrate window with the deposited ice on top was measured. The absorption spectrum of the ice corresponds to the spectrum of the substrate with the ice after subtracting the bare MgF_2 substrate spectrum. In addition, the column density of the ice sample was measured by FTIR in transmittance. The VUV-spectrum and the column density of the ice were therefore monitored in a single experiment for the same ice sample. This improvement allowed us to estimate the VUV-absorption cross section of the ice more accurately. The column density of the deposited ice obtained by FTIR was calculated according to the formula

$$N = \frac{1}{\mathcal{A}} \int_{\rm band} \tau_\nu {\rm d}\nu, \quad (1)$$

where N is the column density of the ice, τ_ν the optical depth of the band, dν the wavenumber differential, in cm^{-1}, and $\mathcal{A}$ is the band strength in cm molecule^{-1}. The integrated absorbance is equal to $0.43 \times \tau$, where τ is the integrated optical depth of the band. The VUV-absorption cross section was estimated according to the Beer-Lambert law,

$$I_{\rm t}(\lambda) = I_0(\lambda) {\rm e}^{-\sigma(\lambda)N}$$
$$\sigma(\lambda) = -\frac{1}{N} \ln\left(\frac{I_{\rm t}(\lambda)}{I_0(\lambda)}\right)$$
$$\text{with} \quad N \approx \frac{N_{\rm i} + N_{\rm f}}{2} \quad (2)$$

where $I_t(\lambda)$ is the transmitted intensity for a given wavelength λ, $I_0(\lambda)$ the incident intensity, N is an average ice column density before ($N_{\rm i}$) and after ($N_{\rm f}$) irradiation in cm^{-2}, and σ is the cross section in cm^2. It is important to notice that the total VUV-flux value emitted by the lamp does not affect the VUV-absorption spectrum of the ice sample, since it is obtained by substracting two spectra to obtain the absorbance in the VUV.

A priori, the VUV-absorption cross section of the ice was not known. Therefore, several measurements for different values of the ice column density were performed to improve the spectroscopy. Table 1 provides the infrared-band position and the band strength used to obtain the column density of each ice component, along with the molecular dipole moment, since the latter has an effect on the intermolecular forces that operate in the ice that distinguish solid spectroscopy from gas phase spectroscopy in the IR and VUV ranges. The gas-phase cross sections published in the literature were also represented for comparison. We note that the majority of the gas-phase cross sections were performed at room temperature. The gas-phase spectrum can vary significantly when the gas sample is cooled to cryogenic temperatures, but it will still differ from the solid-phase spectrum, see Yoshino et al. (1996) and Cheng et al. (2011).

Table 1. Infrared-band positions and strengths ($\mathcal{A}$), deposited column density (N in 10^{15} molec/cm^2) and molecular dipole moment (μ) of the samples used in this work.

Species	Position [cm^{-1}]	$\mathcal{A}$ [cm/molec]	N [$\times 10^{15}$ molec./cm^2)]	μ [D]
CO	2139	$1.1 \pm 0.1 \times 10^{-17}$ [a]	207^{+16}_{-16}	0.11
H_2O	3259	$1.7 \pm 0.2 \times 10^{-16}$ [b]	91^{+7}_{-7}	1.85
CH_3OH	1026	$1.8 \pm 0.1 \times 10^{-17}$ [c]	62^{+5}_{-9}	1.66
NH_3	1067	$1.7 \pm 0.1 \times 10^{-17}$ [c]	67^{+5}_{-8}	1.47
H_2S	2544	$2.0 \pm 0.2 \times 10^{-17}$ [d]	37^{+3}_{-9}	0.95

Notes. Error estimation in the column density is the sum of the error by the band strength, the error by thickness loss for photodesorption, and the MDHL, PMT, and multimeter stabilities. [a] Jiang et al. (1975), [b] calculated for this work, [c] d'Hendecourt & Allamandola (1986), [d] Jiménez-Escobar & Muñoz Caro (2011).

The performance of VUV-spectroscopy inevitably leads to exposure of the sample to irradiation, often causing photodestruction or photodesorption of the ice molecules to some extent during spectral acquisition (e.g., d'Hendecourt et al. 1985, 1986; Bernstein et al. 1995; Gerakines et al. 1995, 1996; Schutte 1996; Sandford 1996; Muñoz Caro et al. 2003, 2010; Dartois 2009; Öberg et al. 2009a,b; Fillion et al. 2012; Fayolle et al. 2011, 2013, and references therein). Photoproduction of new compounds and the decrease of the starting ice column density was monitored by IR spectroscopy. Photodesorption was less intense for the reported species except for CO, in line with the previous works mentioned above; it will also contribute to the decrease of the column density of the ice during irradiation. Photoproduct formation of new compounds is different for each molecule. No photoproducts were detected after the 9 min VUV exposure required for VUV-spectroscopy, except for CH_3OH ice, where product formation was 2%, 6%, 7%, and 8% for CO_2, CH_4, CO, and H_2CO relative to the initial CH_3OH column density estimated by IR spectroscopy. But the VUV-absorption spectrum of CH_3OH was not significantly affected, cf Kuo et al. (2007). Indeed, we show below that the discrete bands of the CO photoproduced in the CH_3OH ice matrix, with an intrinsic absorption higher than methanol in the VUV, are absent from the VUV-absorption spectrum.

Error values for the column density in Table 1 result mainly from the selection of the baseline for integration of the IR absorption band and the decrease of the ice column density due to VUV-irradiation during spectral acquisition. The band strengths were adapted from the literature, and their error estimates are no more than 10% of the reported values (Richey & Gerakines 2012). The solid H_2O band strength in Table 1 was estimated by us using interference fringes in the infrared spectrum for a density of 0.94 g cm^{-3} and a refractive index of 1.3. This estimation gives a value of $1.7 \pm 0.2 \times 10^{-16}$ cm molec^{-1}, different from the Hagen et al. (1985) value (2×10^{-16} cm molec^{-1}). The errors in the column density determined by IR spectroscopy were 16%, 15%, 23%, 19 %, and 32% for solid CO, H_2O, CH_3OH, NH_3, and H_2S ices. The MDHL, photomultiplier tube (PMT), and multimeter stabilities lead to an estimated error of about 6% in

Table 2. Parameter values used to fit the spectra of Gaussian profiles of the different molecular pure ices deposited at 8 K.

Molecule	Center [nm]	*FWHM* [nm]	Area [$\times 10^{-17}$ cm^2 nm]
H_2O	120.0	22.1	12.0
	143.6	17.4	10.8
	154.8	8.0	0.9
CO	127.0	1.27	0.05
	128.9	1.27	0.07
	130.9	1.32	0.14
	132.8	1.27	0.24
	135.2	1.46	0.58
	137.6	1.41	0.95
	140.0	1.62	1.61
	142.8	1.65	1.98
	145.8	2.17	3.16
	148.8	2.24	3.45
	149.7	0.92	0.50
	152.0	2.12	3.09
	153.3	1.34	1.53
	156.3	2.24	3.10
	157.0	1.18	0.56
CH_3OH	118.0	30.6	27.7
	146.6	28.3	16.8
NH_3	121.2	34.1	33.8
	166.6	31.8	14.2

the values of the VUV-absorption cross sections of the ices. The largest error corresponds to H_2S ice, the most VUV photoactive molecule studied in this work. It presents a high photodestruction (Jiménez-Escobar & Muñoz Caro 2011), which leads to a fast decrease in its IR feature. Therefore, VUV-absorption cross-section errors result from the error values estimated above, using the expression

$$\delta(N) = \sqrt{\frac{\delta_i^2 + \delta_j^2 + \delta_k^2 + \ldots + \delta_n^2}{n-1}}. \quad (3)$$

The VUV-absorption cross-section spectra of CO, H_2O, CH_3OH, and NH_3 ices were fitted with Gaussian profiles using the band positions reported in the literature (Lu et al. 2005, 2008; Kuo et al. 2007) as a starting point, see the red traces in Figs. 3–6. Table 2 summarizes the Gaussian profile parameters used to fit the spectra of these ices, deposited at 8 K. H_2S ice displays only a slightly decreasing absorption at longer wavelengths, and Gaussian deconvolution is thus not pertinent. Gaussian fits of the reported molecules were made with an in-house IDL code. The fits reproduce the VUV-absorption cross-section spectra well.

3.1. Solid carbon monoxide

The ground state of CO is $X^1\Sigma^+$ and its bond energy is $E_b(C{-}O) = 11.09$ eV (Okabe 1978).

Figure 3 displays the CO fourth positive band system; it is attributed to the $A^1\Pi \leftarrow X^1\Sigma^+$ system. Table 3 summarizes the transition, band position, and area of each feature at 8 K. We were able to observe twelve bands identified as (0, 0) to (11, 0) where the (0, 0), (1, 0), and (2, 0) bands present a Davydov splitting, in agreement with Mason et al. (2006), Lu et al. (2005), and Brith & Schnepp (1965). Like Mason et al. (2006), we were unable to observe the (12, 0) transition reported by Brith & Schnepp (1965) and Lu et al. (2005), because of the low intensity

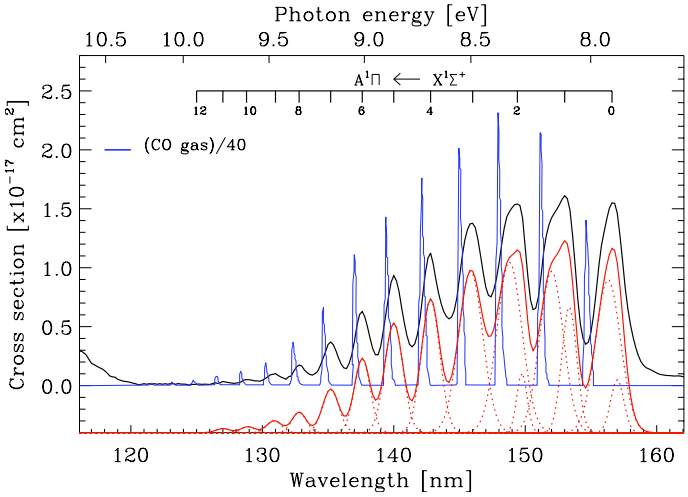

Fig. 3. VUV-absorption cross section as a function of photon wavelength (bottom *X*-axis) and VUV-photon energy (top *X*-axis) of pure CO ice deposited at 8 K, black trace. The blue trace is the VUV-absorption cross-section spectrum of CO gas (divided by a factor of 40 to compare it with CO ice) adapted from Lee & Guest (1981). The fit, red trace, is the sum of 15 Gaussians, dashed trace. It has been vertically offset for clarity.

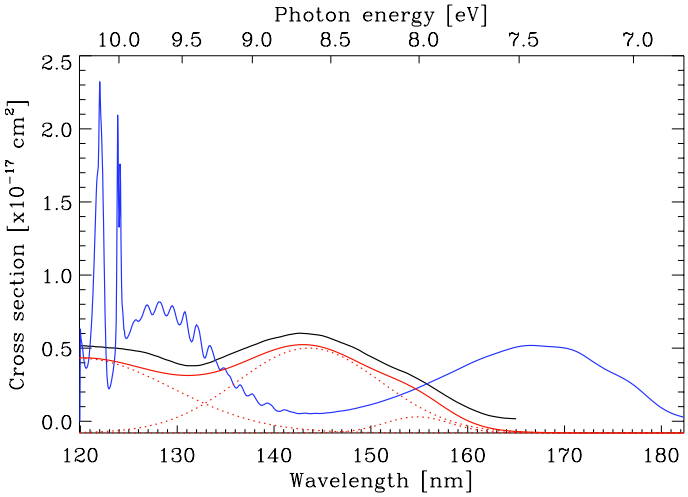

Fig. 4. VUV-absorption cross section as a function of photon wavelength (bottom *X*-axis) and VUV-photon energy (top *X*-axis) of pure H_2O ice deposited at 8 K, black trace. The blue trace is the VUV-absorption cross-section spectrum of gas phase H_2O taken from Mota et al. (2005). The gray area is the measurement error zone. The fit, red trace, is the sum of three Gaussians, dashed trace. It has been vertically offset for clarity.

of this feature. We detected part of the transitions to the excited Rydberg states, $B^1\Sigma^+$, $C^1\Sigma^+$, and $E^1\Pi$ measured by Lu et al. (2005) as a broad band in the 116–121 nm (10.68–10.25 eV) region, despite the decreasing VUV-flux in this region.

The average VUV-absorption cross section has a value of $4.7^{+0.4}_{-0.4} \times 10^{-18}$ cm^2. This value is not very different from the one roughly estimated by Muñoz Caro et al. (2010), 3.8×10^{-18} cm^2 in the 115–170 nm range based on Lu et al. (2005). The total integrated VUV-absorption cross section has a value of $1.5^{+0.1}_{-0.1} \times 10^{-16}$ cm^2 nm ($7.9^{+0.6}_{-0.6} \times 10^{-18}$ cm^2 eV) in the 116–163 nm (10.68–7.60 eV) spectral region. The VUV-absorption of CO ice at 121.6 nm is very low, an upper limit of $\leq 1.1^{+0.8}_{-0.8} \times 10^{-19}$ cm^2 was estimated, while at 157.8 and 160.8 nm the VUV-absorption

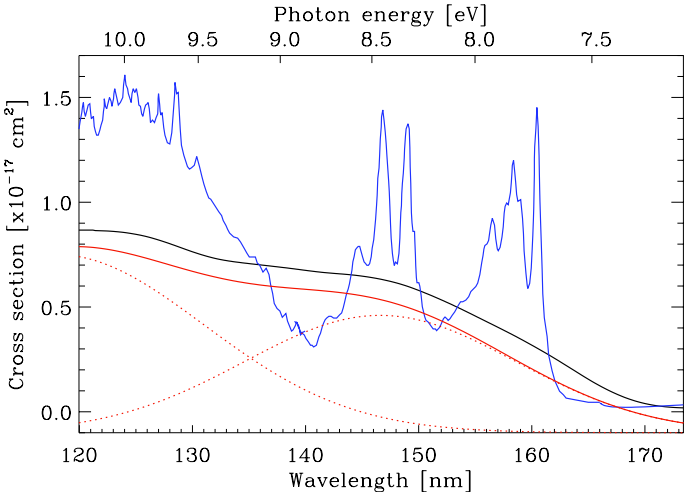

Fig. 5. VUV-absorption cross section as a function of photon wavelength (bottom *X*-axis) and VUV-photon energy (top *X*-axis) of pure CH_3OH ice deposited at 8 K, black trace. The blue trace is the VUV-absorption cross-section spectrum of gas phase CH_3OH adapted from Nee et al. (1985). The fit, red trace, is the sum of two Gaussians, dashed trace. It has been vertically offset for clarity.

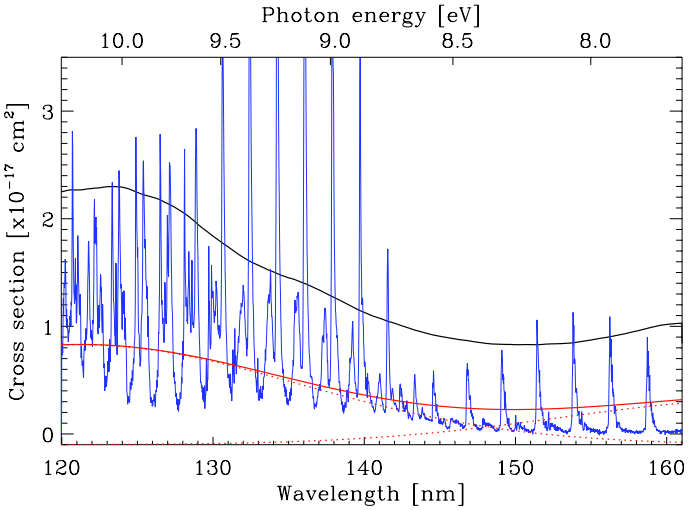

Fig. 6. VUV-absorption cross section as a function of photon wavelength (bottom *X*-axis) and VUV-photon energy (top *X*-axis) of pure NH_3 ice deposited at 8 K, black trace. The blue trace is the VUV-absorption cross-section spectrum of gas phase NH_3 adapted from Cheng et al. (2006) and Wu et al. (2007). The fit, red trace, is the sum of two Gaussians, dashed trace. It has been vertically offset for clarity.

cross sections are $6.6^{+0.5}_{-0.5} \times 10^{-18}$ cm^2 and $0.9^{+0.1}_{-0.1} \times 10^{-18}$ cm^2. The VUV-absorption spectrum of solid CO presents a maximum at 153.0 nm (8.10 eV) with a value of $1.6^{+0.1}_{-0.1} \times 10^{-17}$ cm^2. Table 4 summarizes the transition, band position, and area of each feature present in the CO gas-phase spectrum (blue trace in Fig. 3) adapted from Lee & Guest (1981). The VUV-absorption cross section of CO in the gas phase has an average value of 20.7×10^{-18} cm^2. Based on Lee & Guest (1981), the estimated total integrated VUV-absorption cross section, 2.3×10^{-16} cm^2 nm, is larger than the CO ice value, $1.5 \pm 0.1 \times 10^{-16}$ cm^2 nm. Similar to solid CO, the VUV-absorption cross section of CO gas is very low at 121.6 nm. There are no data available at 157.8 and 160.8 nm, but the absorption is expected to be very low or zero because the first transition (v_0) is centered on 154.5 nm.

Table 3. Transitions observed in the VUV-absorption cross-section spectrum of pure CO ice, deposited at 8 K, in the 115–170 nm range.

	Band peak		Band area	
(v', v")	nm	eV	cm^2 nm	cm^2 eV
11,0	127.0	9.76	8.6×10^{-20}	6.6×10^{-21}
10,0	128.8	9.62	1.6×10^{-19}	1.2×10^{-20}
9,0	131.0	9.46	4.0×10^{-19}	2.9×10^{-20}
8,0	132.8	9.33	7.0×10^{-19}	4.9×10^{-20}
7,0	135.2	9.17	2.6×10^{-18}	1.8×10^{-19}
6,0	137.6	9.01	4.3×10^{-18}	2.8×10^{-19}
5,0	140.0	8.85	7.1×10^{-18}	4.5×10^{-19}
4,0	142.8	8.68	7.6×10^{-18}	4.6×10^{-19}
3,0	146.0	8.49	1.1×10^{-17}	6.5×10^{-19}
2,0	149.4	8.29	1.5×10^{-17}	8.4×10^{-19}
1,0	153.0	8.10	2.5×10^{-17}	1.3×10^{-18}
0,0	156.6	7.91	2.6×10^{-17}	1.3×10^{-18}

Notes. Error margins corresponding to the values in the second and third column are ±0.4 nm and ±0.03 eV. The peak positions agree with previous works, see Mason et al. (2006), Lu et al. (2005), and Brith & Schnepp (1965).

Table 4. Transitions observed in the VUV-absorption cross-section spectrum of pure CO gas based on data adapted from Lee & Guest (1981).

	Band peak		Band area	
(v', v")	nm	eV	cm^2 nm	cm^2 eV
14,0	121.6	10.19	1.5×10^{-19}	1.2×10^{-20}
13,0	123.1	10.07	2.3×10^{-19}	1.9×10^{-20}
12,0	124.7	9.93	6.6×10^{-19}	5.3×10^{-20}
11,0	126.5	9.79	7.5×10^{-19}	5.8×10^{-20}
10,0	128.4	9.65	1.3×10^{-18}	9.7×10^{-20}
9,0	130.3	9.51	2.4×10^{-18}	1.8×10^{-19}
8,0	132.3	9.36	6.5×10^{-18}	4.4×10^{-19}
7,0	134.7	9.20	6.8×10^{-18}	4.8×10^{-19}
6,0	136.9	9.05	1.2×10^{-17}	8.2×10^{-19}
5,0	139.4	8.89	2.1×10^{-17}	1.3×10^{-18}
4,0	142.1	8.72	2.6×10^{-17}	1.7×10^{-18}
3,0	144.9	8.55	2.7×10^{-17}	1.6×10^{-18}
2,0	147.9	8.38	3.3×10^{-17}	1.9×10^{-18}
1,0	151.1	8.20	3.0×10^{-17}	1.6×10^{-18}
0,0	154.4	8.03	2.3×10^{-17}	1.2×10^{-18}

3.2. Solid water

The ground state and bond energy of H_2O are $\tilde{X}^1A_1$ and E_b(H–OH) = 5.1 eV (Okabe 1978).

The VUV-absorption cross-section spectrum of H_2O ice is displayed in Fig. 4. The spectral profile is similar to those reported by Lu et al. (2008) and Mason et al. (2006). The band between 132–163 nm is centered on 142 nm (8.73 eV), in agreement with Lu et al. (2008) and Mason et al. (2006). This band is attributed to the $4a_1$:$\tilde{A}^1B_1 \leftarrow 1b_1$:$\tilde{X}^1A_1$ transition. The VUV-absorption cross section reaches a value of $6.0^{+0.4}_{-0.4} \times 10^{-18}$ cm^{-2} at this peak, which coincides with the spectrum displayed in Fig. 3 of Mason et al. (2006). The H_2O ice spectrum of Lu et al. (2008) presents a local minimum at 132 nm, also visible in Fig. 4. This minimum is not observed in the Mason et al. (2006) data, which is most likely due to the larger scale of their plot. The portion of the band in the 120–132 nm range is attributed to the transition $\tilde{B}^1A_1 \leftarrow \tilde{X}^1A_1$, according to Lu et al. (2008).

The average and the total integrated VUV-absorption cross sections of H_2O ice are $3.4^{+0.2}_{-0.2} \times 10^{-18}$ cm^2 and $1.8^{+0.1}_{-0.1} \times 10^{-16}$ cm^2 nm ($1.2^{+0.1}_{-0.1} \times 10^{-17}$ cm^2 eV) in the 120–165 nm

(10.33−7.51 eV) spectral region. The VUV-absorption cross sections of H_2O ice at 121.6, 157.8, and 160.8 nm are $5.2^{+0.4}_{-0.4} \times 10^{-18}$ cm^2, $1.7^{+0.1}_{-0.1} \times 10^{-18}$ cm^2, and $0.7^{+0.05}_{-0.05} \times 10^{-18}$ cm^2. Gas-phase data from Mota et al. (2005) were adapted for comparison with our solid-phase data, see Fig. 4. Gas and ice data were previously compared by Mason et al. (2006). The VUV-absorption cross section of H_2O in the gas phase has an average value of 3.1×10^{-18} cm^2. H_2O gas data were integrated in the 120−182 nm range, giving a value for the VUV-absorption cross section of 2.3×10^{-16} cm^2 nm (1.4×10^{-17} cm^2 eV), which is higher than the VUV-absorption cross section of solid H_2O. The VUV-absorption cross sections of H_2O gas at 121.6, 157.8, and 160.8 nm are 13.6×10^{-18} cm^2, 3.2×10^{-18} cm^2, and 4.1×10^{-18} cm^2, which is also higher than the solid-phase measurements.

3.3. Solid methanol

The ground state and bond energy of CH_3OH are X^1A' and E_b(H–CH_2OH) = 4.0 eV (Darwent 1970).

Figure 5 shows the VUV-absorption cross section of CH_3OH as a function of wavelength and photon energy. The spectrum profile is similar to the one reported by Kuo et al. (2007), a decreasing continuum for longer wavelengths without distinct local maximum. These authors found three possible broad bands centered on 147 nm (8.43 eV), 118 nm (10.50 eV), and 106 nm (11.68 eV), the latter is beyond our spectral range. We observed the 147 nm peak (associated to the $2^1A'' \leftarrow X^1A'$ molecular transition) as well as part of the 118 nm band (corresponding to the $3^1A'' \leftarrow X^1A'$ molecular transition), but due to the decreasing VUV-flux below 120 nm it was not possible to confirm the exact position of this peak.

The average and the total integrated VUV-absorption cross sections of solid CH_3OH are $4.4^{+0.4}_{-0.7} \times 10^{-18}$ cm^2 and $2.7^{+0.2}_{-0.4} \times 10^{-16}$ cm^2 nm ($1.8^{+0.1}_{-0.3} \times 10^{-17}$ cm^2 eV) in the 120−173 nm (10.33−7.16 eV) spectral region. The VUV-absorption cross sections of CH_3OH ice at 121.6 nm, 157.8 and 160.8 nm are $8.6^{+0.7}_{-1.3} \times 10^{-18}$ cm^2, $3.8^{+0.3}_{-0.6} \times 10^{-18}$ cm^2, and $2.9^{+0.2}_{-0.4} \times 10^{-18}$ cm^2. Gas phase data from Nee et al. (1985) were used for comparison with our solid-phase spectrum, see Fig. 5. Pure gas and solid CH_3OH, and CH_3OH in Ar or Kr matrices were compared by Kuo et al. (2007). CH_3OH gas has a vibrational peak profile throughtout the 120−173 nm range, which is absent from in CH_3OH ice. The VUV-absorption cross section of CH_3OH in the gas phase has an average value of 8.9×10^{-18} cm^2. CH_3OH gas data were integrated in the 120−173 nm range, giving a value for the VUV-absorption cross section of 3.7×10^{-16} cm^2 nm (2.5×10^{-17} cm^2 eV), which is higher than the VUV-absorption cross section ($2.7^{+0.2}_{-0.4} \times 10^{-16}$ cm^2 nm) for solid CH_3OH. The VUV-absorption cross sections of CH_3OH gas at 121.6 nm, 157.8, and 160.8 nm are 13.2×10^{-18} cm^2, 9.9×10^{-18} cm^2, and 8.6×10^{-18} cm^2, which are also higher than the ice-phase measurements.

3.4. Solid ammonia

The ground state of NH_3 is $\tilde{X}^1A_1$ and its bond energy is E_b(H–NH_2) = 4.4 eV (Okabe 1978).

Figure 6 displays the VUV-absorption cross section of NH_3 as a function of the photon wavelength and photon energy. It presents a continuum with two broad absorption bands between 120−151 nm (10.33−8.21 eV) and 151−163 nm (8.21−7.60 eV) in this wavelength region, without narrow bands associated to vibrational structure. Mason et al. (2006) found a broad band centered on 177 nm (7.00 eV) in the 146−225 nm (5.50−8.50 eV) spectral range. Lu et al. (2008) observed the same feature centered on 179 nm (6.94 eV). We observed only a portion of this feature because of the low VUV-flux of the MDHL in the 163−180 nm (7.60−6.88 eV) spectral range. This band is associated to the $\tilde{A}^1A_2'' \leftarrow \tilde{X}^1A_1$ molecular transition. The minimum we observed at 151 nm (8.21 eV) is the same as in the above-cited works. At this minimum, the VUV-absorption cross section reaches a value of $3.3 \pm 0.2 \times 10^{-18}$ cm^2, higher than the 1.9×10^{-18} cm^2 value reported in Fig. 10 of Mason et al. (2006). We also obtained a higher value at 128.4 nm (9.65 eV), $8.1 \pm 0.5 \times 10^{-18}$ cm^2 compared with 3.8×10^{-18} cm^2 by Mason et al. (2006). This difference is most likely due to the different method employed to estimate the ice column density, infrared spectroscopy or laser interferometry. In addition, a broad band centered on 121.2 nm (10.23 eV) was observed, in agreement with Lu et al. (2008), probably associated to the $\tilde{B} \leftarrow \tilde{X}$ molecular transition.

The average and the total integrated VUV-absorption cross sections of solid NH_3 are $4.0^{+0.3}_{-0.5} \times 10^{-18}$ cm^2 and $2.2^{+0.2}_{-0.3} \times 10^{-16}$ cm^2 nm ($1.5^{+0.1}_{-0.2} \times 10^{-17}$ cm^2 eV) in the 120−161 nm (10.33−7.70 eV) spectral region. The VUV-absorption cross sections of NH_3 ice at 121.6 nm, 157.8 and 160.8 nm are $9.1^{+0.7}_{-1.1} \times 10^{-18}$ cm^2, $3.8^{+0.3}_{-0.5} \times 10^{-18}$ cm^2, and $4.1^{+0.3}_{-0.5} \times 10^{-18}$ cm^2. Gas-phase data from Cheng et al. (2006) and Wu et al. (2007) were adapted, see Fig. 5. At least qualitatively, our result is compatible with Mason et al. (2006). The VUV-absorption cross section of NH_3 in the gas phase has an average value of 6.1×10^{-18} cm^2. NH_3 gas data were integrated in the 120−161 nm range, giving a value of 2.5×10^{-16} cm^2 nm (1.8×10^{-17} cm^2 eV), slightly higher than the VUV-absorption cross section of solid NH_3 ($2.2^{+0.2}_{-0.3} \times 10^{-16}$ cm^2 nm). The VUV-absorption cross sections of NH_3 gas at 121.6, 157.8 and 160.8 nm are 9.8×10^{-18} cm^2, 0.1×10^{-18} cm^2, and 0.3×10^{-18} cm^2; these values are lower than the ice-phase measurements, except for the Ly-α photon wavelength (121.6 nm).

3.5. Solid hydrogen sulfide

The ground state and bond energy of H_2S are $\tilde{X}^1A_1$ and E_b(H–SH) = 3.91 eV (Okabe 1978).

Figure 7 shows the VUV-absorption cross section of H_2S as a function of the wavelength and photon energy. Owing to the high VUV-absorption of solid H_2S, very thin ice samples were deposited to obtain a proper VUV-spectrum. H_2S gas has a nearly constant VUV-absorption cross section in the 120−150 nm (10.33−8.26 eV) range, between 150−180 nm (8.26−6.88 eV) it decreases, and in the 180−250 nm (6.88−4.95 eV) region it presents a maximum at 187 nm (6.63 eV), see Okabe (1978). The VUV-absorption cross section of H_2S is almost constant in the 120−143 nm (10.33−8.67 eV) range and decreases in the 143−173 nm (8.67−7.16 eV) range, with a maximum at 200 nm (6.19 eV) according to Feng et al. (1999). The $^1B_1 \leftarrow {}^1A_1$ molecular transition was identified at 139.1 nm (8.91 eV) by Price & Simpson (1938) and confirmed by Gallo & Innes (1975).

The total integrated VUV-absorption cross section of H_2S ice has a value of $1.5^{+0.1}_{-0.3} \times 10^{-15}$ cm^2 nm ($4.3^{+0.3}_{-1.0} \times 10^{-16}$ cm^2 eV) in the 120−160 nm (10.33−7.74 eV) spectral region. The VUV-absorption cross sections of the same ice at 121.6, 157.8, and 160.8 nm are $4.2^{+0.3}_{-1.0} \times 10^{-17}$ cm^2, $3.4^{+0.3}_{-0.8} \times 10^{-17}$ cm^2, and $3.3^{+0.3}_{-0.8} \times 10^{-17}$ cm^2. Gas-phase data from Feng et al. (1999) were adapted, see Fig. 7. The spectrum of the solid is almost constant,

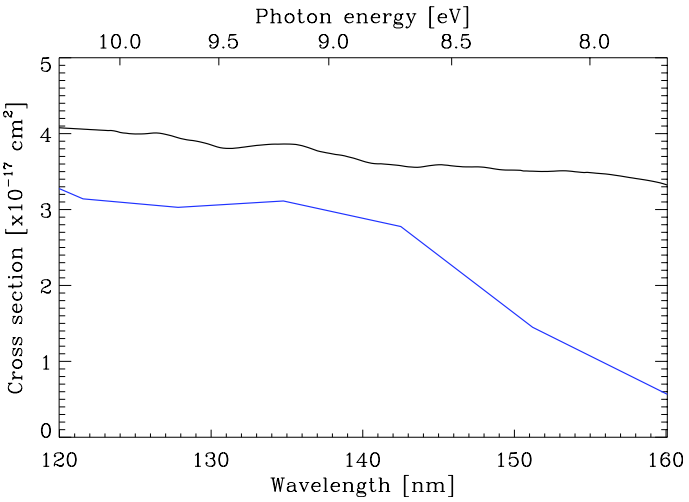

Fig. 7. VUV-absorption cross section as a function of wavelength (bottom X-axis) and photon energy (top X-axis) of pure H_2S ice deposited at 8 K, black trace. The blue trace is the VUV-absorption cross-section spectrum of gas phase H_2S adapted from Feng et al. (1999).

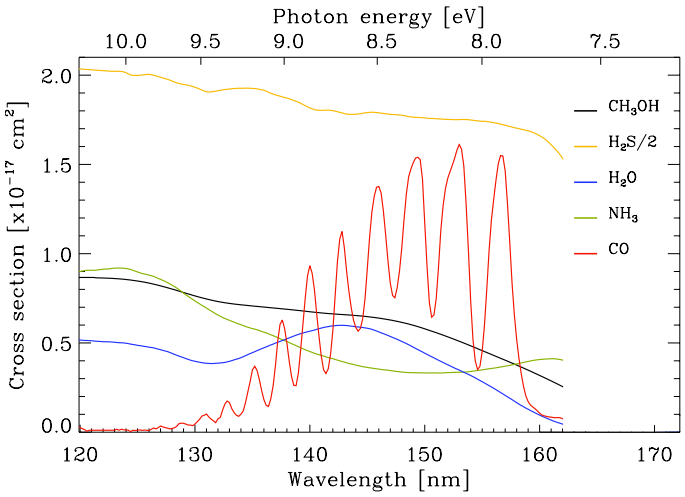

Fig. 8. VUV-absorption cross section as a function of wavelength (bottom x-axis) and photon energy (top x-axis) of all the pure ice species studied in this work, deposited at 8 K.

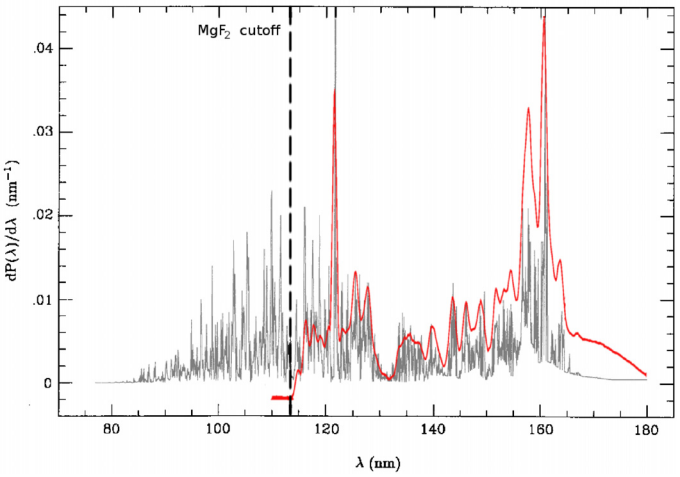

Fig. 9. Calculated spectrum of ultraviolet photons created in the interior of dense molecular clouds by impact excitation of molecular hydrogen by cosmic ray ionization, adapted from Gredel et al. (1989), in the background. VUV-emission spectrum of the MDHL used in this work, red foreground trace.

only a slight decrease is observed as the wavelength increases. The gas-phase spectrum presents an abrupt decrease in the cross section starting near 140 nm, according to Feng et al. (1999). In contrast to the Okabe (1978) data, this spectrum of the gas shows no vibrational structure, probably because of its low resolution. The average VUV-absorption cross section of H_2S gas reported by Feng et al. (1999), 3.1×10^{-17} cm^2, disagrees by one order of magnitude with the $3-4 \times 10^{-18}$ cm^2 value of Okabe (1978). We estimated a value of $3.9^{+0.3}_{-0.9} \times 10^{-17}$ cm^2 for the solid in the same range, which is close to the Feng et al. (1999) gas-phase value.

H_2S gas data were integrated in the 120−160 nm range, giving a value of 10.2×10^{-16} cm^2 nm (8.0×10^{-17} cm^2 eV), which is lower than the VUV-absorption cross section of solid H_2S. The VUV-absorption cross sections of H_2S gas at 121.6, 157.8, and 160.8 nm are 31.0×10^{-18} cm^2, 7.9×10^{-18} cm^2, and 4.9×10^{-18} cm^2, which are also lower than the solid-phase values reported above.

3.6. Comparison between all the ice species

Figure 8 shows a comparison of the VUV-absorption cross section for all the ice species deposited at 8 K, represented in the same linear scale. The most absorbing molecule is H_2S. H_2O has the lowest average absorption in this range. All the represented species absorb VUV-light significantly in the 120−163 nm (10.33−7.60 eV) range, only the CO absorption is negligible at the Ly-α wavelength. Except for CO, the absorption of the reported ice species in the H_2 molecular emission region between 157−161 nm is lower than the Ly-α absorption. Table 5 summarizes the comparison between the VUV-absorption cross sections of all the species in the gas and solid phase.

4. Astrophysical implications

Far-ultraviolet observations of IC 63, an emission/reflection nebula illuminated by the B0.5 IV star γCas, with the *Hopkins* Ultraviolet Telescope (HUT) on the central nebular position, have revealed a VUV-emission spectrum very similar to the spectrum of our VUV-lamp, see Fig. 4 of France et al. (2005), which means that the VUV-spectrum that interacts with the ice sample mimicks the molecular hydrogen photoexcitation observed toward this photodissociation region (PDR) in the local interstellar medium. This spectrum is similar to that emitted by the MDHL with a H_2 pressure of 0.2 mbar.

Ice mantle build-up takes place in cold environments such as dark cloud interiors, where the radiation acting on dust grains is the secondary UV field produced by cosmic ray ionization of H_2. These are the conditions mimicked in our experiments: low density and low temperature, and UV photons impinging on ice mantles. The secondary UV field calculated by Gredel et al. (1989) is very similar to the emission spectrum of our lamp, see Fig. 9, except for photons with wavelengths shorter than about 114 nm, which are not transmitted by the MgF_2 window used as interface between the MDHL and the ISAC set-up.

The reported VUV-absorption cross sections allow a more quantitative study of photon absorption in ice mantles. Based on our data, the VUV-light reaching an interstellar ice mantle must have an energy higher than 7.00, 7.60, and 7.08 eV, to be absorbed by solid CO, H_2O, and CH_3OH, respectively. The full absorption spectrum in the VUV measured by other authors provides an absorption threshold above 6.20 and 5.16 eV for NH_3

Table 5. Comparison between the VUV-absorption cross sections in the 120−160 nm range of all the pure species in the gas and solid (deposited at 8 K) phase.

	Species	Total Int. [$\times 10^{-16}$ cm^2 nm]	Avg.	Ly-α	LBS	121.6 nm [$\times 10^{-18}$ cm^2]	157.8 nm	160.8 nm
Solid phase	CO	$1.5^{+0.1}_{-0.1}$	$4.7^{+0.4}_{-0.4}$	$0.1^{+0.01}_{-0.01}$	$11^{+0.9}_{-0.9}$	$0.1^{+0.01}_{-0.01}$	$6.6^{+0.5}_{-0.5}$	$0.9^{+0.07}_{-0.07}$
	H_2O	$1.8^{+0.1}_{-0.1}$	$3.4^{+0.2}_{-0.2}$	$5.1^{+0.4}_{-0.4}$	$4.0^{+0.3}_{-0.3}$	$5.2^{+0.4}_{-0.4}$	$1.7^{+0.1}_{-0.1}$	$0.7^{+0.05}_{-0.05}$
	CH_3OH	$2.2^{+0.2}_{-0.3}$	$4.4^{+0.4}_{-0.7}$	$6.7^{+0.5}_{-1.0}$	$6.4^{+0.5}_{-1.0}$	$8.6^{+0.7}_{-1.3}$	$3.8^{+0.3}_{-0.6}$	$2.9^{+0.2}_{-0.4}$
	NH_3	$2.2^{+0.1}_{-0.3}$	$4.0^{+0.3}_{-0.5}$	$9.1^{+0.7}_{-1.1}$	$3.6^{+0.3}_{-0.5}$	$9.1^{+0.7}_{-1.1}$	$3.8^{+0.3}_{-0.5}$	$4.1^{+0.3}_{-0.5}$
	H_2S	15^{+1}_{-3}	39^{+3}_{-9}	41^{+3}_{-10}	34.0^{+3}_{-8}	42^{+3}_{-10}	34^{+3}_{-8}	33^{+3}_{-8}
Gas phase	CO	2.3	20.7	–	–	–	–	–
	H_2O	2.3	3.1	–	–	13.6	3.2	4.1
	CH_3OH	3.4	8.2	–	–	13.6	8.5	10.0
	NH_3	2.5	6.1	–	–	9.8	0.1	0.3
	H_2S	10.2	31.0	–	–	31.0	7.9	4.9

Notes. Total Int. is the total integrated VUV-absorption cross section in this range, Avg. is the average VUV-absorption cross section. Ly-α and LBS are the average VUV-absorption cross sections in the 120.8−122.6 nm and 132−162 nm range normalized by the photon flux. The last three columns are the VUV-absorption cross sections at wavelengths 121.6 nm (corresponding to the maximum intensity of the Ly-α peak), 157.8 and 160.8 nm (main peaks of the Lyman band system).

Table 6. Penetration depth, expressed as absorbing column density, of the different pure ice species deposited at 8 K, corresponding to an absorbed photon flux of 95% and 99%.

Species	95% photon absorption			99% photon absorption		
	Ly-α ($\times 10^{17}$	Avg. molecule	Max. cm^{-2})	Ly-α ($\times 10^{17}$	Avg. molecule	Max. cm^{-2})
CO	≥150	6.4	1.9	≥230	9.8	2.9
H_2O	5.8	8.3	4.9	8.9	13.0	7.7
CH_3OH	3.5	5.7	3.4	5.4	8.7	5.3
NH_3	3.3	5.5	3.2	5.1	8.5	5.0
H_2S	0.73	0.81	0.73	1.1	1.2	1.1

Notes. Ly-α corresponds to the cross section at the Ly-α wavelength, 121.6 nm; in the case of CO, the upper limit in the cross section leads to a lower limit in the absorbing column density. Avg. corresponds to the average value of the cross section in the 120−160 nm range. Max. corresponds to the maximum value of the cross section in the same wavelength range. Errors in the penetration depth correspond to those estimated for the VUV-absorption cross sections of the different ices.

and H_2S, respectively, see Mason et al. (2006) and Feng et al. (1999).

The ice penetration depth of photons with a given wavelength, or the equivalent absorbing ice column density of a species in the solid phase, can be calculated from the VUV-absorption cross section following Eq. (2). Table 6 summarizes the penetration depth of the ice species for an absorbed photon flux of 95% and 99% using the cross section value at Ly-α, the average value of the cross section in the 120−160 nm range, and the maximum value of the cross section in the same range.

The VUV-absorption of ice mantles is low compared with that of the dust grain cores, and therefore difficult to observe directly, but it is an essential parameter quantitatively for studing the photoprocessing and photodesorption of molecular species in the ice mantle. The desorbing photoproducts can be detected in observations of the gas phase. The reported measurements of the cross sections are thus needed to estimate the absorption of icy grain mantles in the photon range where molecules are photodissociated or photodesorbed, which often leads to the formation of photoproducts. These results can be used as input in models that predict the processing of ice mantles that are exposed to an interstellar VUV-field. They can be used, for instance, to predict the gas phase abundances of molecules photodesorbed from the ice mantles, as we discuss below.

There is a clear correspondence between the photodesorption rates of CO ice measured at different photon energies (Fayolle et al. 2011) and the VUV-absorption spectrum of CO ice (Lu et al. 2009, this work) for the same photon energies. This indicates that photodesorption of some ice species like CO and N_2 is mainly driven by a desorption induced by electronic transition (DIET) process (Fayolle et al. 2011, 2013). The lowest photodesorption reported by Fayolle et al. (2011) at the Ly-α wavelength (121.6 nm) is $<6 \times 10^{-3}$ molecules per incident photon, coinciding with the low VUV-absorption at this wavelength in Fig. 3, and the maximum in the photodesorption occurs approximately at ∼151.2 nm, near the most intense VUV-absorption band, see Fig. 3. The photodesorption rate per absorbed photon in the $[\lambda_i, \lambda_f]$ wavelength range, R^{abs}_{ph-des}, can differ significantly from the photodesorption rate per incident photon, R^{inc}_{ph-des}. It can be estimated as follows:

$$R^{abs}_{ph-des} = \frac{\Delta N}{I_{abs}} \quad \text{and} \quad R^{inc}_{ph-des} = \frac{\Delta N}{I_0}$$

$$R^{abs}_{ph-des} = \frac{I_0}{I_{abs}} R^{inc}_{ph-des}, \tag{4}$$

where

$$I_{abs} = \sum_{\lambda_i}^{\lambda_f} I_0(\lambda) - I(\lambda) = \sum_{\lambda_i}^{\lambda_f} I_0(\lambda)(1 - e^{-\sigma(\lambda)N}),$$

Table 7. VUV-absorption cross sections for different irradiation energies.

Irrad. energy eV	σ cm^2	R^{inc}_{ph-des} molec./photon$_{inc}$	R^{abs}_{ph-des} molec./photon$_{abs}$
10.2	1.1×10^{-19}	$6.9 \pm 2.4 \times 10^{-3}$	12.5 ± 4.4
9.2	2.8×10^{-18}	$1.3 \pm 0.91 \times 10^{-2}$	0.9 ± 0.6
† 8.2	9.3×10^{-18}	5×10^{-2}	1.1
8.6	4.7×10^{-18}	$5.1 \pm 0.2 \times 10^{-2}$	2.5 ± 0.1

Notes. R_{inc} values correspond to Fayolle et al. (2011), except for 8.6 eV, which is the average photon energy of our MDHL and the corresponding value of the cross section is the average VUV-absorption cross section of pure CO ice, deposited at 8 K, in the 120–160 nm range. R^{abs}_{ph-des} values for a column density of about 5 ML, i.e. where the absorbed photons contribute to a photodesorption event (Muñoz Caro et al. 2010; Fayolle et al. 2011). † Peak yield value at ~8.2 eV, see Fayolle et al. (2011).

and ΔN is the column density decrease for a given irradiation time in molecules cm^{-2} s^{-1}, I_0 is the total photon flux emitted (Fayolle et al. 2011 reports $\sim 1.7 \times 10^{14}$ photons cm^{-2} s^{-1}, in our experiments $\sim 2.0 \times 10^{14}$ photons cm^{-2} s^{-1}), I_{abs} is the total photon flux absorbed by the ice, $I_0(\lambda)$ is the photon flux emitted at wavelength λ, $\sigma(\lambda)$ is the VUV absorption cross section at the same wavelength, and N is the column density of the ice sample.

Fayolle et al. (2011) reported $R^{inc}_{ph-des} = 5 \times 10^{-2}$ molecules per incident photon for monochromatic ~8.2 eV light irradiation of a 9–10 ML ice column density of CO. We also estimated the value of $R^{inc.}_{ph-des}$ in our CO irradiation experiment using the MDHL continuum emission source with an average photon energy of 8.6 eV; this gave a value of $5.1 \pm 0.2 \times 10^{-2}$ for an ice column density of 223 ML, in agreement with Muñoz Caro et al. (2010). Therefore, similar values of R^{inc}_{ph-des} are obtained using either, monochromatic or continuum emission sources, provided that the photon energy of the former is near the average photon energy of the latter, this is discussed below. Using Eq. (4), we estimated the R^{abs}_{ph-des} values in both experiments; they are summarized in Table 7 for a column density of 5 ML (only the photons absorbed in the top 5 ± 1 ML participate in the photodesorption) for three monochromatic photon energies in the Fayolle et al. (2011) work, selected to coincide with Lyman-α (10.2 eV), the maximum cross section (9.2 eV energy), and the monochromatic energy of 8.2 eV, that is, the one closer to the average photon energy of the MDHL at 8.6 eV.

Irradiation of CO ice using our VUV-lamp, with a broadband energy distribution and mean energy of ~8.6 eV, gives similar R^{inc}_{ph-des} values, but different R^{abs}_{ph-des} values than irradiation with a ~8.2 eV energy monochromatic light source (Fayolle et al. 2011). This suggests that in this particular case, the photodesorption rate per incident photon does not depend much on the photon energy distribution, but this coincidence is only by chance, since the corresponding R^{abs}_{ph-des} values differ significantly.

The properties of individual molecular componentes of interstellar ice analogs have been studied over the years (e.g., Sandford et al. 1988; Sandford & Allamandola 1990; Gerakines et al. 1996; Escribano et al. 2013). Our VUV-absorption spectra can be directly applied to astrophysical icy environments practically made of a single compound, for example, either CO_2 or H_2O largely dominate the composition of different regions at the south pole of Mars (Bibring et al. 2004). Nevertheless, interstellar ice mantles are either thought to be a mixture of different species or to present a layered structure (e.g., Gerakines et al. 1995; Dartois et al. 1999; Pontoppidan et al. 2008; Boogert et al. 2011; Öberg et al. 2011; Kim et al. 2012). Our study on pure ices can be used to estimate the absorption of multilayered ice mantles, but a priori, it cannot be extrapolated to ice mixtures. A follow-up of this work will include ice mixtures and VUV-spectroscopy at ice temperatures above 8 K.

5. Conclusions

Several conclusions can be drawn from our experimental work; they are summarized as follows:

- The combination of infrared (FTIR) spectroscopy in transmission for measuring the deposited ice column density and VUV-spectroscopy allowed us to determine more accurate VUV-absorption cross-section values of interstellar ice analogs with an error within 16%, 15%, 23%, 19%, and 32% for CO, H_2O, CH_3OH, NH_3, and H_2S. The errors are mainly caused by the ice column density decrease due to VUV-irradiation during VUV spectral acquisition.

- For the first time, the VUV-absorption cross sections of CO, CH_3OH and H_2S were measured for the solid phase, with average VUV-absorption cross sections of $4.7^{+0.4}_{-0.4} \times 10^{-18}$ cm^2, $4.4^{+0.4}_{-0.7} \times 10^{-18}$ cm^2, and $39^{+3}_{-9} \times 10^{-18}$ cm^2. The total integrated VUV-absorption cross sections are $1.5^{+0.1}_{-0.1} \times 10^{-16}$ cm^2 nm, $2.7^{+0.2}_{-0.4} \times 10^{-16}$ cm^2 nm, and $1.5^{+0.1}_{-0.3} \times 10^{-15}$ cm^2 nm. Our estimated values of the average VUV-absorption cross sections of H_2O and NH_3 ices $3.4^{+0.2}_{-0.2} \times 10^{-18}$ cm^2 and $4.0^{+0.3}_{-0.5} \times 10^{-18}$ cm^2, are comparable with those reported by Mason et al. (2006), which were measured using a synchrotron as the emission source.

- The ice samples made of molecules such as H_2O, CH_3OH, and NH_3 present broad absorption bands and similar average VUV-absorption cross sections between $3.4^{+0.2}_{-0.2} \times 10^{-18}$ cm^2 and $4.4^{+0.4}_{-0.7} \times 10^{-18}$ cm^2, see Fig. 8. But H_2S ice, which also displays a continuum spectrum, presents about four times more absorption than the other molecules in the same VUV range.

- Solid CO displays discrete VUV-absorption bands and very low absorption at the Ly-α wavelength. But the other solid samples present high absorption at the Ly-α wavelength.

- For the H_2O, CH_3OH, and NH_3 species, the VUV-absorption range and the total integrated VUV-absorption cross section in the gas phase is larger than the solid phase. An exception is H_2S.

- The main emission peaks of the MDHL occur at 121.6 nm (Lyman-α), 157.8 nm and 160.8 nm (molecular H_2 bands), see Fig. 2. It is still a common mistake in the molecular astrophysics community to consider the MDHL as a pure Ly-α photon source. As we mentioned, the lamp VUV-spectrum affects the photochemistry but not the VUV-spectroscopy in a direct way, since the VUV-emission spectrum was subtracted to measure the ice absorption in the same energy range.

- Monitoring of the photon energy distribution and the stability of the irradiation source is important for studing ice photoprocesses.

– The results are satisfactory and demonstrate the viability of the MDHL, which commonly used in irradiation experiments, as a source for VUV spectroscopy of solid samples. This method to perform VUV-spectroscopy does not require a synchrotron facility and can be used routinely in the laboratory.

– Our estimates of the VUV-absorption cross sections of polar ice molecules can be used as input in models that simulate the photoprocessing of ice mantles present in cold environments, such as dense cloud interiors and circumstellar regions. The data reported in this paper can be applied to estimate the absorption of layered ice mantles, but not to ices built up with different species that are intimately mixed.

Acknowledgements. This research was financed by the Spanish MICINN under projects AYA2011−29375 and CONSOLIDER grant CSD2009−00038. This work was partially supported by NSC grants NSC99−2112-M-008−011-MY3 and NSC99−2923-M-008−011-MY3, and the NSF Planetary Astronomy Program under Grant AST-1108898.

References

Bibring, J. -P., Langevin, Y., Poulet, F., et al. 2004, Nature, 428, 627
Boursey, E., Chandrasekharan, V., Gürtler, P., et al. 1978, Phys. Rev. Lett., 41, 1516
Boogert, A. C. A., Huard, T. L., Cook, A. M., et al. 2011, ApJ, 729, 92
Brith, M., & Schnepp, O. 1965, Molecular Phys., 9, 473
Cecchi-Pestellini, C., & Aiello, S. 1992, MNRAS, 258, 125
Chen, Y.-J., Chu, C.-C, Lin, Y.-C, et al. 2010, Adv. Geosci., 25, 259
Chen, Y.-J., Chuang, K.-Y., & Muñoz Caro, G. M. 2013, ApJ, in press
Cheng, B.-M., Lu, H.-C., Chen, H.-K., et al. 2006, ApJ, 647, 1535
Cheng, B.-M., Chen, H.-F., Lu, H.-C., et al. 2011, ApJS, 196, 6
Collings, M.P., Anderson, M.A., Chen, R., et al. 2004, MNRAS, 354, 1133
Dalgarno, A., & Stephens, T. L. 1970, ApJ, 160, L107
Darwent, B. de B. 1970, Bond Dissociation Energies in Simple Molecules, National Standard Reference Data System, 31, 70−602101
Dartois, E. 2009, ASP Conf. Ser., 414, 411
Dartois, E., Demyk, K., d'Hendecourt, L., & Ehrenfreund, P. 1999, A&A, 351, 1066
Dartois, E., Pontoppidan, K., Thi, W.-F., & Muñoz Caro, G. M. 2005, A&A, 444, L57
Dawes, A., Mukerji, R. J., Davis, M. P., et al. 2007, J. Chem. Phys., 126, 244711
d'Hendecourt, L. B., Allamandola, L. J., & Greenberg, J. M. 1985. A&A, 152, 130
d'Hendecourt, L. B., Allamandola, L. J., Grim, R. J. A., & Greenberg, J. M. 1986. A&A, 158, 119
Ehrenfreund, P., & van Dishoeck, E. F. 1998, Adv. Space Res., 21, 15
Escribano, R., Muñoz Caro, G. M., Cruz-Diaz, G. A., Rodríguez-Lazcano, Y., & Maté, B. 2013, PNAS, 110, 12899
Fayolle, E. C., Bertin, M., Romanzin, C., et al. 2011, ApJ, 739, L36
Fayolle, E. C., Bertin, M., Romanzin, C., et al. 2013, A&A, 556, A122
Feng, R., Cooper, G., & Brion, C. E. 1999, Chem. Phys., 244, 127
Fillion, J.-H., Bertin, M., Lekic, A., et al. 2012, EAS Publ. Ser., 58, 307
France, K., Andersson, B.-G., McCandliss, S. R., & Feldman, P. D. 2005, ApJ, 628, 750
Gallo, A. R., & Innes, K. K. 1975, J. Mol. Spectrosc., 54, 472
Gerakines, P. A., Schutte, W. A., Greenberg, J. M., & van Dishoeck, E. F. 1995. A&A, 296, 810
Gerakines, P. A., Schutte, W. A., & Ehrenfreund, P. 1996, A&A, 312, 289
Gibb, E. L., Whittet, D. C. B., Boogert, A. C. A., & Tielens, A. G. G. M. 2004, ApJ, 151, 35
Gredel, R., Lepp, S., & Dalgarno, A. 1989, ApJ, 347, 289
Hudson, R. D., & Carter, V. L. 1968, J. Opt. Soc. Am., 58, 227
Inn, E. C. Y. 1954, Spectrochimica Acta, 7, 65
Jiang, G. J., Person, W. B., & Brown, K. G. 1975, J. Chem. Phys., 75, 4198
Jiménez-Escobar, A., & Muñoz Caro, G. M. 2011, A&A, 536, A11
Kim, H. J., Evans II, N. J., Dunham, M. M., Lee, J. -E., & Pontoppidan, K. M. 2012, ApJ, 758, 38
Knez, C., Boogert, A. C. A., Pontoppidan, K. M., et al. 2005, ApJ, 635, L145
Kuo, Y.-P., Lu, H.-C., Wu, Y.-J., Cheng, B.-M., & Ogilvie, J. F. 2007, Chem. Phys. Lett., 447, 168
Lee, L. C., & Guest, J. A. 1981, J. Phys. B: At. Mol. Phys., 14, 3415
Lu, H.-C., Chen, H.-K., Cheng, B.-M., Kuo, Y.-P., & Ogilvie, J. F. 2005, J. Phys. B: At. Mol. Opt. Phys., 38, 3693
Lu, H.-C., Chen, H.-K., Cheng, B.-M., & Ogilvie, J. F. 2008, Spectrochimica Acta Part A, 71, 1485
Mason, N. J., Dawes, A., Holton, P. D., et al. 2006, Faraday Discussions, 133, 311
Monahan, K. M., & Walker, W. C. 1974, J. Chem. Phys., 61, 3886
Mota, R., Parafita, R., Giuliani, A., et al. 2005, Chem. Phys. Lett., 416, 152
Mumma, M. J., & Charnley, S. B. 2011, Annu. Rev. Astro. Astrophys., 49, 471
Muñoz Caro, G. M., Jiménez-Escobar, A., Martín-Gago, J.Á., et al. 2010, A&A, 522, A108
Nee, J. B., Suto, M., & Lee, L. C. 1985, Chem. Phys., 98, 147
Öberg, K. I., Garrod, R. T., van Dishoeck, E. F., & Linnartz, H. 2009a. A&A, 504, 891
Öberg, K. I., Linnartz, H., Visser, R., & van Dishoeck, E. F. 2009b. ApJ, 693, 1209
Öberg, K. I., Boogert, A. C. A., Pontoppidan, K. M., et al. 2011, ApJ, 740, 109
Okabe, H. 1978, Photochemistry of small molecules (New York: John Wiley & Sons)
Pontoppidan, K. M., Boogert, A. C. A., Fraser, H. J., et al. 2008, ApJ, 678, 1005
Price, W. C., & Simpson, D. M. 1938, Proc. Roy. Soc. London A, 165, 272
Richey, C. R., & Gerakines, P. A. 2012, ApJ, 759, 74
Samson, J. A. R., & Ederer, D. L. 2000, Vacuum Ultaviolet Spectroscopy (Elsevier Inc.)
Sandford, S. A. 1996, ASP Conf. Ser., 97, 29
Sandford, S. A., & Allamandola, L. J. 1990, ApJ, 355, 357
Sandford, S. A., Allamandola, L. J., Tielens, A. G. G. M., & Valero, G. J. 1988, ApJ, 329, 498
Schutte, W. A. 1996, Molecules in Astrophysics: Probes and Processes, IAU Symp., 178, 1
Smith, P. L., Rufus, L., Yoshino, K., & Parkinson, W. H. 2002, in NASA Laboratory Astrophysics Workshop, NASA/CP-2002−21186, ed. F. Salama, 158
Sternberg, A. 1989, ApJ, 347, 863
Wu, Y.-J., Lu, H.-C., Chen, H.-K., & Cheng, B.-M. 2007, J. Chem. Phys., 127, 154311
Wu, Y.-J., Wu, C. Y. R., Chou S.-L., et al. 2012, ApJ, 746, 175
Yoshino, K., Esmond, J. R., Sun, Y., et al. 1996, J. Quant. Spectrosc. Radiat. Transf., 55, 53